RSC Advances

PAPER

View Article Online
View Journal | View Issue

Cite this: *RSC Adv.*, 2017, **7**, 6762

Single-component Eu^{3+}–Tb^{3+}–Gd^{3+}-grafted polymer with ultra-high color rendering index white-light emission†

Lin Liu,[a] Guorui Fu,[a] Baoning Li,[a] Xingqiang Lü,*[a] Wai-Kwok Wong[b] and Richard A. Jones[c]

Received 13th November 2016
Accepted 30th December 2016

DOI: 10.1039/c6ra26724f

www.rsc.org/advances

Through an approach of pre-coordination and following terpolymerization from vinyl-functionalized complex monomers [Ln(TTA)$_3$(4-VB-PBI)] (Ln = Eu, **2**; Ln = Tb, **3** and Ln = Gd, **4**; HTTA = 2-thenoyltrifluoroacetonate; 4-VB-PBI = 1-(4-vinylbenzyl)-2-(pyridin-2-yl)-1*H*-benzo[*d*]imidazole) with methyl methacrylate, the first example of a single-component Eu^{2+}–Tb^{3+}–Gd^{3+}-grafted polymer **Poly(MMA-*co*-2-*co*-3-*co*-4)** was obtained. Moreover, control of an optimal dye content for suppressing Tb^{3+} to Eu^{3+} energy transfer and exciton formation provides new perspectives for hetero-Ln^{3+}-grafted polymers as featured in **Poly(MMA-*co*-2-*co*-3-*co*-4)** with color-tuning to direct white-light (Commission International De L'Eclairage coordinates of $x = 0.322$, $y = 0.331$; corrected color temperature of 5979 K; and color rendering index up to 94), including a highly luminous efficiency of 17.8%.

Introduction

White-light-emitting materials are receiving considerable research attention because of their wide applications[1] in solid-state lighting, back-lighting for liquid-crystal display and full-color flat-panel display. Until now, even though several white-light-emitting materials reliant on inorganic phosphors[2] or nano-crystals,[3] organic dyes,[4] polymers,[5] transition-metallic complexes[6] and transition-metal-grafted polymers[7] have been studied extensively, organo-lanthanide (Ln^{3+}) sources are still of special interest. This interest can be attributed to the uniqueness of Ln^{3+} emitting specific, narrow line-like emission over a long lifetime. In this context, in contrast to the distinctive drawbacks of low thermal stability and/or phase separation for Ln^{3+}-complexes[8] or their doping systems[9] and the inherent defect of poor mechanical properties for Ln^{3+}-related metal–organic frameworks (MOFs),[10] Ln^{3+}-grafted polymers should be considered.[11] A polymeric matrix endows exceptional thermal stability, good mechanical strength and excellent film-forming property. Moreover, a single-component strategy for Ln^{3+}-grafted polymers[12] capable of white-light production renders easier fabrication and better color rendition as compared with a common multi-component strategy.[13] Nonetheless, realization of high luminous efficiencies for single-component homo- or hetero-Ln^{3+}-grafted polymers remains a challenge. Especially from the viewpoint of high-quality white-light, an ultra-high color rendering index (CRI; >90) single-component system ideal for fabricating white polymeric light-emitting diodes or other optoelectronic devices has not been reported.

White-light-emitting single-component homo-[12a,12b] or hetero-Ln^{3+}-grafted polymers[12c] are regularly constructed through post-coordination from the first-prepared coordination site-retained polymer skeletons with europium ion (Eu^{3+}) and/or terbium ion (Tb^{3+})-complex units. However, due to the usual wrapping of coordination sites by polymeric backbones or branched-chains, discerning the localized circumstance and stoichiometry of Ln^{3+} within them is difficult. The solution can have recourse to another feasible approach[12d] of pre-coordination and copolymerization where, by establishing Eu^{3+} and/or Tb^{3+}-complex primary-color monomers with definite micro-environments in advance, the chromophore content is "fine-tuned" through control of the desired feed ratios of monomers during copolymerization. An alternative more worthy of consideration is smooth supplementation of the color-compensatory deficiency from terpolymerization of co-monomers. Nevertheless, it still suffers from an unmanageable Tb^{3+} to Eu^{3+} energy transfer in Eu^{3+}–Tb^{3+}–grafted polymers[12c] or intangible aggregation-induced exciton formation in Eu^{3+}- or Tb^{3+}-containing metallopolymers,[12a,12b] which is fatal to white-light modulation[14] and makes obtaining an ultra-high CRI value difficult.[12d,15] Our conceptual strategy of molecular dispersal of all-incorporated chromophores within a polymeric matrix should be promising. That is, the Ln^{3+}-complex primary-

[a]*School of Chemical Engineering, Shaanxi Key Laboratory of Degradable Medical Material, Northwest University, Xi'an 710069, Shaanxi, China*

[b]*Department of Chemistry, Hong Kong Baptist University, Waterloo Road, Kowloon Tong, Hong Kong, China*

[c]*Department of Chemistry and Biochemistry, The University of Texas at Austin, 1 University Station A5300, Austin, TX 78712-0165, USA*

† Electronic supplementary information (ESI) available. CCDC 1494131. For ESI and crystallographic data in CIF or other electronic format see DOI: 10.1039/c6ra26724f

color components are separated to effectively suppress Tb^{3+} to Eu^{3+} energy transfer or exciton formation through an optimal grafting concentration, and their simultaneous emission gives rise to continuous broad spectra for direct white-light. Herein, with terpolymerization of vinyl-functionalized complex monomers [Ln(TTA)$_3$(4-VB-PBI)] (Ln = Eu, **2**; Ln = Tb, **3** and Ln = Gd, **4**) with methyl methacrylate (MMA), the first example of a polymethyl methacrylate (PMMA)-supported and Eu^{2+}–Tb^{3+}–Gd^{3+}-grafted single-component polymer **Poly(MMA-*co*-2-*co*-3-*co*-4)** was obtained. Through control of a safe grafting concentration, color-tuning to white-light with an ultra-high CRI was also expected from integration of Eu^{3+}-red-light, Tb^{3+}-green-light and ligand-centered Gd^{3+}-incorporated blue-light. Moreover, its comparison relative to the polymer blend **Poly(MMA-*co*-2)@Poly(MMA-*co*-3)@Poly(MMA-*co*-4)** was also explored.

Experimental section

High-performance liquid chromatography (HPLC)-grade tetrahydrofulan (THF) or acetonitrile (MeCN) was purchased from Fisher Scientific and purified over solvent columns prior to use. Other solvents were used as received from Sigma-Aldrich and stored over 3 Å-activated molecular sieves. MMA was washed twice with aqueous NaOH (5%, wt) and twice with distilled water, followed by drying over anhydrous $MgSO_4$ and distillation over CaH_2 under a N_2 atmosphere at reduced pressure. Azobis(isobutyronitrile) (AIBN) was purified by recrystallization twice from absolute MeOH prior to use. Other chemicals were commercial products of reagent grade and used without further purification. Elemental analyses were performed on a PerkinElmer 240C elemental analyzer. Infrared spectra were recorded on a Nicolet Nexus-670 FT-IR spectrophotometer with KBr pellets in the region 4000–400 cm^{-1}. ^1H NMR spectra were recorded on a Bruker Plus 400 spectrometer with $SiMe_4$ as the internal standard in DMSO-d_6 at room temperature. Electrospray ionization mass spectrometry (ESI-MS) was performed on a Finnigan LCQ^{DECA} XP HPLC-MS$_n$ mass spectrometer with a mass to charge (m/z) range of 4000 using a standard electrospray ion source and $CHCl_3$ or MeCN as solvent. Electronic absorption spectra in the UV/vis region and diffuse reflection (DR) spectra were recorded with a Cary 300 UV spectrophotometer. Visible emission and excitation spectra were collected by a combined fluorescence lifetime and steady-state spectrometer (FLS-980) with a 450 W Xe lamp. Excited-state decay times were obtained by the same spectrometer but with a μF900 Xe lamp. The luminescent absolute overall quantum yield (Φ_{em} or Φ_{Ln}^{L}) in solution or solid state was determined by the same spectrometer using a 450 W Xe lamp and an integrating sphere. Gel permeation chromatography (GPC) analyses of polymers were performed using a Waters 1525 binary pump coupled to a Waters 2414 refractive index detector with HPLC THF as the eluant on American Polymer Standard linear mixed bed packing columns (particle size, 10 μm). GPC was calibrated using polystyrene standards. X-ray photoelectron spectroscopy (XPS) was carried out on a PHI 5700 XPS system equipped with a dual Mg X-ray source and monochromatic Al X-ray source complete with depth profile and angle-resolved capabilities. Powder X-ray diffraction (PXRD) patterns were recorded on a D/Max-IIIA diffractometer with graphite-monochromatized Cu Kα radiation (λ = 1.5418 Å). Thermal properties were characterized using thermogravimetric (TG) analyses and differential scanning calorimetry (DSC) on a NETZSCH TG 209 instrument under nitrogen at a heating rate of 10 °C min^{-1}.

Synthesis of the precursor 2-(pyridine-2-yl)-1*H*-benzo[*d*] imidazole (HPBI)

The benzimidazole-based organic precursor HPBI was synthesized from the reaction of 1,2-diaminobenzene (2.75 g, 25 mmol) with 2-pyridinecarboxaldehyde (2.68 g, 25 mmol) in the presence of *p*-toluenesulfonic acid (2.27 mmol, 0.40 g) according to a well-established procedure.[16] Yield: 4.10 g (84%). Calc. for $C_{12}H_9N_3$: C, 73.83; H, 4.65; N 21.52%. Found: C, 73.80; H, 4.69; N, 21.54%. ^1H NMR (400 MHz, DMSO-d_6): δ (ppm) 13.13 (s, 1H, –NH), 8.75 (d, 1H, –Py), 8.33 (t, 1H, –Py), 8.01 (t, 1H, –Py), 7.71 (d, 1H, –Py), 7.54 (t, 2H, –Ph), 7.24 (t, 2H, –Ph).

Synthesis of the vinyl-functionalized ancillary ligand 4-VB-PBI (4-VB-PBI = 1-(4-vinylbenzyl)-2-(pyridin-2-yl)-1*H*-benzo[*d*] imidazole)

To the solution of HPBI (2.00 g, 10 mmol) in absolute DMSO (20 mL), tetraethylammonium bromide (0.20 g, 10 mmol) was added, and the mixture was reacted at RT. After 2 h, an aqueous solution (5 mL) of KOH (0.67 g, 12 mmol) was added dropwise, and the resulting mixture stirred at RT for another 2 h. Solid 1-(chloromethyl)-4-vinylbenzene (1.80 g, 12 mmol) was added and the resultant mixture continuously stirred at RT overnight. Then, the mixture was poured into deionized water (200 mL) to give a white precipitate. The crude product was filtered and further dissolved into absolute EtOH (30 mL) to give a white polycrystalline solid by evaporation at RT. Yield: 2.40 g (76%). Calc. for $C_{21}H_{17}N_3$: C, 81.00; H, 5.50; N, 13.49%. Found: C, 79.46; H, 5.58; N, 13.42%. FT-IR (KBr, cm^{-1}): 3048 (w), 3000 (w), 2987 (w), 1744 (w), 1716 (w), 1610 (m), 1589 (m), 1568 (m), 1510 (m), 1463 (m), 1440 (s), 1407 (w), 1390 (s), 1350 (w), 1331 (m), 1275 (m), 1267 (w), 1259 (w), 1210 (w), 1165 (m), 1148 (w), 1111 (m), 1097 (m), 1083 (w), 1046 (m), 1017 (w), 992 (m), 979 (m), 910 (m), 824 (s), 791 (m), 774 (m), 764 (m), 738 (vs), 700 (m), 626 (m), 612 (m), 578 (w), 562 (w), 543 (w). ^1H NMR (400 MHz, DMSO-d_6): δ (ppm) 8.70 (d, 1H, –Py), 8.37 (d, 1H, –Py), 8.01 (t, 1H, –Py), 7.77 (m, 1H, –Py), 7.59 (m, 1H, –Ph), 7.52 (m, 1H, –Ph), 7.34 (d, 2H, –Ph), 7.28 (m, 2H, –Ph), 7.10 (d, 2H, –Ph), 6.63 (m, 1H, –CH=C), 6.22 (s, 2H, –CH_2), 5.73 (d, 1H, =CH_2), 5.19 (d, 1H, =CH_2). ESI-MS (in $CHCl_3$) m/z: 312.39 (100%), $[M - H]^+$.

Synthesis of a series of vinyl-containing complex monomers [Ln(TTA)$_3$(4-VB-PBI)] (Ln = La, 1; Ln = Eu, 2; Ln = Tb, 3; Ln = Gd, 4)

To a stirred MeOH solution (15 mL) of the ligand 2-thenoyltrifluoroacetonate (HTTA; 132 mg, 0.6 mmol) in the presence of an equimolar amount of NaOH (24 mg, 0.6 mmol), another aqueous solution (10 mL) of $LnCl_3 \cdot 6H_2O$ (0.2 mmol; Ln = La, 71 mg; Ln = Eu, 73 mg; Ln = Tb, 75 mg or Ln = Gd, 74 mg) was added, and precipitation occurred immediately, respectively.

Under vigorous stirring at RT for 12 h, each of the off-white precipitates was separated by filtration, and washed with deionized water and absolute CH_2Cl_2. After drying at 45 °C under vacuum, each of the solid products was added to a mixed solvent (30 mL; EtOH and petroleum ether, v/v = 3 : 1), and solid 4-VB-PBI (62 mg, 0.2 mmol) was added, then the resultant mixture was continuously stirred at RT for another 12 h. The respective clear-yellow solution was filtered, and left to stand at RT for several days to give the pale-yellow microcrystalline products of complex monomers **1–4**, respectively.

For **1**: yield: 167 mg (75%). Calc. for $C_{45}H_{29}F_9LaN_3O_6S_3$: C, 48.53; H, 2.62; N, 3.77%. Found: C, 48.29; H, 2.69; N, 3.75%. FT-IR (KBr, cm^{-1}): 3093 (w), 2989 (w), 2901 (w), 1614 (m), 1596 (s), 1535 (s), 1507 (m), 1476 (m), 1457 (m), 1411 (s), 1355 (m), 1298 (s), 1288 (sh), 1246 (m), 1229 (m), 1182 (s), 1134 (vs), 1122 (m), 1083 (w), 1060 (m), 1034 (w), 1010 (w), 989 (w), 932 (m), 913 (w), 859 (m), 836 (w), 785 (s), 746 (s), 717 (s), 692 (w), 680 (m), 640 (m), 605 (w), 578 (w), 542 (w), 532 (w). ^{1}H NMR (400 MHz, DMSO-d_6): δ (ppm) 8.69 (d, 1H, –Py), 8.38 (d, 1H, –Py), 8.01 (t, 1H, –Py), 7.62 (s, 7H, –Py and –Th), 7.58 (t, 1H, –Ph), 7.52 (t, 1H, –Ph), 7.34 (d, 2H, –Ph), 7.28 (m, 2H, –Ph), 7.10 (d, 5H, –Ph and –Th), 6.62 (m, 1H, –CH=C), 6.22 (s, 2H, $-CH_2$), 6.15 (s, 3H, –CH), 5.74 (d, 1H, $=CH_2$), 5.19 (d, 1H, $=CH_2$). ESI-MS (in MeCN) *m*/*z*: 1114.82 (100%), $[M - H]^+$.

For **2**: yield: 176 mg (78%). Calc. for $C_{45}H_{29}F_9EuN_3O_6S_3$: C, 47.96; H, 2.59; N, 3.73%. Found: C, 47.83; H, 2.67; N, 3.64%. FT-IR (KBr, cm^{-1}): 3096 (w), 2988 (w), 2902 (w), 1615 (m), 1597 (s), 1537 (s), 1505 (m), 1478 (m), 1458 (m), 1411 (s), 1354 (m), 1302 (s), 1290 (sh), 1246 (m), 1230 (m), 1184 (s), 1134 (vs), 1121 (m), 1083 (w), 1061 (m), 1036 (w), 1015 (w), 1010 (sh), 989 (w), 934 (m), 914 (m), 859 (m), 836 (w), 785 (s), 746 (s), 717 (s), 693 (w), 681 (m), 642 (m), 605 (w), 581 (m), 545 (w), 535 (w). ESI-MS (in MeCN) *m*/*z*: 1127.88 (100%), $[M - H]^+$.

For **3**: yield: 161 mg (71%). Calc. for $C_{45}H_{29}F_9TbN_3O_6S_3$: C, 47.67; H, 2.58; N, 3.71%. Found: C, 47.53; H, 2.71; N, 3.65%. FT-IR (KBr, cm^{-1}): 3093 (w), 2975 (w), 2902 (w), 1611 (m), 1598 (s), 1537 (s), 1507 (m), 1476 (m), 1459 (m), 1412 (s), 1356 (m), 1304 (s), 1291 (w), 1246 (m), 1230 (m), 1186 (s), 1134 (vs), 1125 (m), 1082 (w), 1061 (m), 1036 (w), 1014 (w), 1010 (w), 992 (w), 932 (m), 914 (w), 859 (m), 836 (w), 785 (s), 768 (m), 746 (s), 719 (s), 693 (w), 680 (m), 641 (m), 605 (w), 581 (m), 543 (w), 531 (w). ESI-MS (in MeCN) *m*/*z*: 1134.84 (100%), $[M - H]^+$.

For **4**: yield: 159 mg (70%). Calc. for $C_{45}H_{29}F_9GdN_3O_6S_3$: C, 47.74; H, 2.58; N, 3.71%. Found: C, 47.61; H, 2.69; N, 3.66%. FT-IR (KBr, cm^{-1}): 3094 (w), 2988 (w), 2901 (w), 1618 (m), 1598 (s), 1536 (s), 1505 (m), 1477 (m), 1459 (m), 1428 (w), 1411 (s), 1354 (m), 1303 (s), 1291 (sh), 1246 (m), 1230 (m), 1184 (s), 1133 (vs), 1126 (m), 1083 (w), 1061 (m), 1035 (w), 1014 (w), 1010 (sh), 989 (w), 934 (m), 914 (w), 859 (m), 835 (w), 785 (s), 768 (m), 746 (s), 717 (s), 690 (w), 681 (m), 643 (m), 601 (w), 580 (m), 547 (w), 534 (w). ESI-MS (in MeCN) *m*/*z*: 1133.17 (100%), $[M - H]^+$.

Synthesis of homo-Ln^{3+}-grafted polymers poly(MMA-*co*-[Ln(TTA)$_3$(4-VB-PBI)]) (Ln = La, 1; Eu, 2; Tb, 3; Gd, 4)

The homogeneous copolymerization of MMA and each of the vinyl-containing complex monomers **1–4** activated with AIBN (1.5 mol% of MMA) was carried out in a Fisher-Porter glass reactor and protected by a reduced N_2 atmosphere. A mixture of MMA (9.5 mmol, 1 mL) and one of the complex monomers **1–4** at a stipulated feed molar ratio (100 : 1, 200 : 1, 400 : 1 or 600 : 1) in the presence of AIBN initiator (1.5 mol% of MMA) was dissolved in dry THF (30 mL), and the respective resultant mixture heated to 60 °C with continuous stirring for 48 h under a reduced N_2 atmosphere. All the reaction mixtures remained clear throughout the polymerization. After cooling to room temperature, each viscous mixture was diluted with dry THF (20 mL) and precipitated with absolute diethyl ether (50 mL) thrice. The resulting solid products were collected by filtration and dried at 45 °C under vacuum to constant weight, respectively.

For **Poly(MMA-*co*-1)** (200 : 1): yield: 87%. FT-IR (KBr, cm^{-1}): 2992 (w), 2951 (w), 1728 (vs), 1681 (w), 1480 (m), 1448 (m), 1436 (m), 1387 (m), 1369 (w), 1270 (m), 1242 (m), 1193 (m), 1148 (s), 1074 (w), 1065 (m), 1057 (w), 988 (w), 967 (w), 913 (w), 842 (w), 812 (w), 803 (w), 750 (m), 720 (w), 673 (w), 656 (m), 630 (m). ^{1}H NMR (400 MHz, DMSO-d_6): δ (ppm) 8.70 (b, 1H, –Py), 8.37 (b, 1H, –Py), 8.02 (b, 2H, –Py), 7.76 (b, 4H, –Ph and –Th), 7.54 (d, 3H, –Ph), 7.28 (b, 4H, –Ph), 6.97 (m, 6H, –Ph), 6.18 (b, 5H, $-CH_2$ and –CH), 3.55 (s, 260H, –COOMe), 2.85 (b, 1H, –CH), 1.82 (m, 175H, $-CH_2$), 1.32 (b, 2H, $-CH_2$), 0.93 (m, 260H, $-CH_3$).

For **Poly(MMA-*co*-2)** (100 : 1, 200 : 1, 400 : 1 or 600 : 1): yield: 84% (100 : 1); 88% (200 : 1); 91% (400 : 1); 93% (600 : 1). FT-IR (KBr, cm^{-1}): 2994 (w), 2951 (w), 1728 (vs), 1680 (w), 1483 (m), 1449 (m), 1436 (m), 1387 (m), 1369 (w), 1270 (m), 1242 (m), 1192 (m), 1149 (s), 1084 (w), 1065 (m), 1052 (w), 987 (w), 965 (w), 911 (w), 841 (w), 813 (w), 805 (w), 750 (m), 722 (w), 672 (w), 653 (m), 630 (m).

For **Poly(MMA-*co*-3)** (100 : 1, 200 : 1, 400 : 1 or 600 : 1): yield: 82% (100 : 1); 86% (200 : 1); 90% (400 : 1); 92% (600 : 1). FT-IR (KBr, cm^{-1}): 2994 (w), 2951 (w), 1727 (vs), 1681 (w), 1483 (m), 1448 (m), 1435 (m), 1387 (m), 1369 (w), 1272 (m), 1242 (m), 1193 (m), 1149 (s), 1075 (w), 1065 (m), 1057 (w), 986 (w), 967 (w), 914 (w), 842 (w), 810 (w), 805 (w), 750 (m), 720 (w), 673 (w), 654 (m), 630 (m).

For **Poly(MMA-*co*-4)** (200 : 1): yield: 85%. FT-IR (KBr, cm^{-1}): 2990 (w), 2952 (w), 1726 (vs), 1681 (w), 1482 (m), 1448 (m), 1436 (m), 1386 (m), 1370 (w), 1271 (m), 1242 (m), 1192 (m), 1149 (s), 1076 (w), 1066 (m), 1057 (w), 988 (w), 967 (w), 913 (w), 843 (w), 810 (w), 803 (w), 750 (m), 721 (w), 673 (w), 654 (m), 631 (m).

Synthesis of polymers' blend Poly(MMA-*co*-2)@Poly(MMA-*co*-3)@Poly(MMA-*co*-4) with different doping mass ratios (1 : 7 : 4, 1 : 7 : 8 or 1 : 7 : 12)

A mixture of **Poly(MMA-*co*-2)**, **Poly(MMA-*co*-3)** and **Poly(MMA-*co*-4)** obtained from AIBN-initiated copolymerization of MMA and one of the complex monomers **2–4** at the same stipulated feed molar ratio (200 : 1) was dissolved in absolute $CHCl_3$ (30 mL) with one of the mass ratios (1 : 7 : 4, 1 : 7 : 8 or 1 : 7 : 12) to form a clear solution, and each of the resulting solutions was stirred under a reduced N_2 atmosphere at RT for 36 h. After precipitation with absolute diethyl ether (50 mL) thrice, each of the resultant solid products was collected by filtration and dried at 45 °C under vacuum to constant weight. For **Poly(MMA-*co*-2)**

@Poly(MMA-*co*-3)@Poly(MMA-*co*-4): yield: 95% (1 : 7 : 4); 94% (1 : 7 : 8) or 96% (1 : 7 : 12). FT-IR (KBr, cm^{-1}): 2993 (w), 2951 (w), 1728 (vs), 1482 (w), 1448 (m), 1436 (m), 1387 (w), 1270 (m), 1242 (m), 1193 (m), 1148 (s), 1062 (w), 989 (w), 968 (w), 917 (w), 841 (w), 828 (w), 816 (w), 811 (w), 797 (w), 783 (w), 776 (w), 750 (m), 732 (w), 722 (w), 701 (w), 685 (w), 673 (w), 660 (w), 643 (m), 627 (m).

Synthesis of Eu^{3+}–Tb^{3+}–Gd^{3+}-grafted polymers Poly(MMA-*co*-2-*co*-3-*co*-4) with a stipulated feed molar ratio of 200 : 1[2/3/4] = 1 : 7 : 4, 1 : 7 : 8 or 1 : 7 : 12

Poly(MMA-*co*-2-*co*-3-*co*-4) with a stipulated feed molar ratio and different monomer-mixed molar ratios (200 : 1[**2**/**3**/**4**] = 1 : 7 : 4, 1 : 7 : 8 or 1 : 7 : 12) was prepared in the same way as shown for **Poly(MMA-*co*-2)** (200 : 1) except that complex monomers **2–4** with different mixed molar ratios ([**2**/**3**/**4**] = 1 : 7 : 4, 1 : 7 : 8 or 1 : 7 : 12) were used instead of complex monomer **2**. For **Poly(MMA-*co*-2-*co*-3-*co*-4)** (200 : 1[**2**/**3**/**4**] = 1 : 7 : 4, 1 : 7 : 8 or 1 : 7 : 12): yield: 86% (200 : 1[**2**/**3**/**4**] = 1 : 7 : 4); 87% (200 : 1[**2**/**3**/**4**] = 1 : 7 : 8) or 85% (200 : 1[**2**/**3**/**4**] = 1 : 7 : 12). FT-IR (KBr, cm^{-1}): 2989 (w), 2953 (w), 2902 (w), 1730 (vs), 1484 (m), 1448 (m), 1436 (m), 1393 (m), 1387 (m), 1271 (m), 1242 (m), 1193 (m), 1148 (s), 1075 (w), 1066 (m), 1059 (w), 989 (w), 967 (w), 911 (w), 843 (w), 812 (w), 800 (w), 751 (m), 720 (w), 673 (w), 648 (m), 629 (m). XPS quantitative results of Ln^{3+} molar ratios: $Eu^{3+}/Tb^{3+}/Gd^{3+}$ = 1 : 6.97 : 3.93 *vs.* 1 : 7 : 4; 1 : 7.02 : 7.96 *vs.* 1 : 7 : 8; 1 : 6.98 : 11.95 *vs.* 1 : 7 : 12.

Results and discussion

Synthesis and characterization of vinyl-containing complex monomers 1–4

As shown in Scheme 1, the vinyl-functionalized ancillary ligand 4-VB-PBI was synthesized from the nucleophilic replacement reaction of 1-(chloromethyl)-4-vinylbenzene with the benzimidazole-based precursor HPBI in the presence of KOH in a yield of 76%. Furthermore, through self-assembly of the deprotonated β-diketonate ligand $(TTA)^-$, $LnCl_3 \cdot 6H_2O$ (Ln = La, Eu, Tb or Gd) and the ancillary ligand 4-VB-PBI in a molar ratio of 3 : 1 : 1, a series of vinyl-containing complex monomers [Ln(TTA)$_3$(4-VB-PBI)] (Ln = La, **1**; Ln = Eu, **2**; Ln = Tb, **3** or Ln = Gd, **4**) was obtained, respectively. The ancillary ligand 4-VB-PBI and its four complex monomers **1–4** were well-characterized by EA, FT-IR, ^{1}H NMR and ESI-MS. In the FT-IR spectra of **1–4**, the similar and combined absorption characteristics of the coordinated precursor 4-VB-PBI and (TTA)-ligand are exhibited, and the remaining two characteristic absorptions at 1611–1618 and 1121–1126 cm^{-1} assigned to the respective ν(=CH) vibration and the γ(=CH) vibration of the active vinyl group are also observed. With respect to the ^{1}H NMR spectrum (Fig. 1S†) of anti-ferromagnetic La^{3+}-based complex monomer **1**, besides a stipulated proton molar ratio (3 : 1) of $(TTA)^-$ to 4-VB-PBI, the proton resonances (δ = 6.62, 5.74 and 5.19 ppm) of the terminal functional vinyl group remain identical to those (δ = 6.63, 5.73 and 5.19 ppm) of 4-VB-PBI despite the coordination of La^{3+}. Moreover, ESI-MS spectra of the series of complex monomers **1–4** display similar patterns and exhibit a strong mass peak at *m*/*z* 1114.82 (**1**), 1127.88 (**2**), 1134.84 (**3**) or 1133.17 (**4**) assigned to the major species $[M - H]^+$ of complex monomers **1–4**, respectively, indicating that the respective discrete tris-β-diketonate mononuclear unit is retained in the corresponding dilute MeCN solution.

Molecular structure of [Gd(TTA)$_3$(4-VB-PBI)] (**4**) as a representative of complex monomers **1–4** was obtained by single-crystal X-ray diffraction analysis, with crystallographic data shown in Tables 1 and 2S.† Complex monomer **4** crystallizes in the space group $P\bar{1}$ with the asymmetric unit consisting of one Gd^{3+}, three deprotonated $(TTA)^-$ ligands and one ancillary ligand 4-VB-PBI. As shown in Fig. 1, the central Gd^{3+} (Gd1) is eight-coordinate, whereby three deprotonated $(TTA)^-$ ligands with a similar *O*,*O*′-chelate mode and one ancillary ligand 4-VB-PBI with a *N*,*N*′-chelate mode coordinate to one Gd^{3+} (Gd1) in a square anti-prismatic geometry, resulting in formation of a typical tris-β-diketonate binary mononuclear host structure.[17] The six Gd–O bond lengths (2.334(4)–2.367(4) Å) are slightly shorter than those (2.525(5)–2.602(6) Å) of the two Gd–N bonds, and the coordination of Gd^{3+} endows almost co-planar characteristics of the thiophene ring with the *O*,*O*′-chelate ring for each deprotonated $(TTA)^-$ ligand and the benzimidazole ring, and the pyridine ring with the *N*,*N*′-chelate ring for the ancillary ligand 4-VB-PBI. These observations, together with involvement

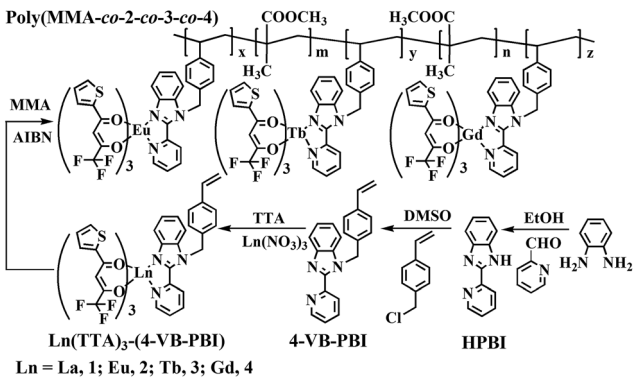

Scheme 1 Reaction scheme for the synthesis of the vinyl-functionalized complex monomers **1–4** and Eu^{3+}–Tb^{3+}–Gd^{3+}-grafted polymer **Poly(MMA-*co*-2-*co*-3-*co*-4)**.

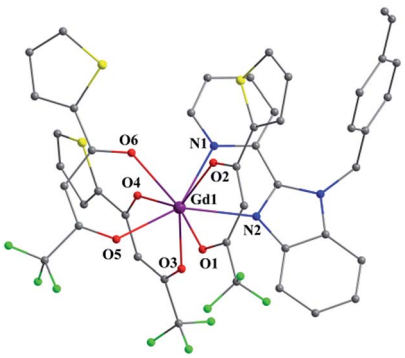

Fig. 1 Perspective drawing of complex monomer [Gd(TTA)$_3$(4-VP-PBI)] (**4**); H atoms have been omitted for clarity.

of the CF_3-group in each $(TTA)^-$ ligand, promote spin–orbit coupling to effectively sensitize Ln^{3+}-based luminescence. It is worth noting that the retained vinyl functional group characteristic of a typical C=C bond length of 1.2996(12) Å from 4-VB-PBI in complex monomer **4** renders each of the complex monomers active for the following copolymerization.

Photophysical properties and energy-transfer process of vinyl-containing complex monomers 2–4 in solution

The photophysical properties of complex monomers **2–4** were investigated in dilute MeCN solution at RT or 77 K, and summarized in Fig. 2 and 2S.† The similar and combined ligands-centered absorption spectra of 202–204, 260–264 and 324–326 nm for complex monomers **2–4** in the UV-visible region are observed (Fig. 2S†), where the lowest energy absorptions should be attributed to the π–π* transitions of $(TTA)^-$ and 4-VB-PBI ligands. For complex monomer **2**, photo-luminescence (λ_{ex} = 380 nm) exhibits just the Eu^{3+}-centered characteristic emissions ($^5D_0 \rightarrow {}^7F_J, J = 0$–4) shown in Fig. 2, giving a bright color-pure red-light with a Commission International De L'Eclairage (CIE) chromatic coordinate (0.665, 0.334). However, use of Tb^{3+} in the replacement endows complex monomer **3** dual emissions (CIE chromatic coordinate 0.174, 0.187) composed of both ligands-based residual blue-light emission at 434 nm and Tb^{3+}-centered characteristic green-light ($^5D_4 \rightarrow {}^7F_J$, J = 6, 5, 4, 3). Moreover, the outstanding color-pure red-light **2** can also be testified by a long Eu^{3+}-centered ($^7F_2$, λ_{em} = 613 nm) lifetime of 312 μs and an inspiring Φ^L_{Eu} of 47.0% within all the reported $(TTA)_3$–Eu^{3+}-complexes.[18] With regard to **3**, two-centered species decay with a fluorescence lifetime (2.7 ns) of the ligands-based residual emission and a phosphorescence lifetime 143 μs of Tb^{3+}, respectively, whereas its large optical absorbance of the $(TTA)^-$ and 4-VB-PBI involved renders an attractive Φ^L_{Tb} of 6.8% for **3**.

To further address the sensitization mechanism of complex monomers **2–3**, their iso-structural Gd^{3+}-based complex monomer **4**, as a suitable reference, endows study of chromophore luminescence in the absence of energy transfer because Gd^{3+} has no energy levels below 32 000 cm^{-1}, and so cannot accept any energy from the excited state of the chromophore.[19] Different from the typical fluorescent blue-light (λ_{em} = 432 nm, τ = 3.4 ns and Φ^L_{em} = 3.5%) assigned to the intra-ligand π–π* transition at RT and belonging to the perturbation luminescence of Gd^{3+} to the ligand, complex monomer **4** exhibits 0–0 transition phosphorescence (λ_{em} = 480 nm and τ = 7.6 μs) at 77 K, from which the triplet (^{3}π–π*) energy level at 20 833 cm^{-1} is obtained with regard to the singlet (^{1}π–π*) energy level (25 974 cm^{-1}) estimated by the lower wavelength of its UV-visible absorbance edge. Therefore, in addition to the slightly larger energy gap ΔE^1 (^{1}π–π* to ^{3}π–π*, 5141 cm^{-1}) than 5000 cm^{-1} endowing the effective intersystem crossing process according to Reinhouldt's empirical rule,[20] the ligands-based ^{3}π–π* energy level (20 833 cm^{-1}) lies above the energies of the main emitting levels of $^5D_0$ (17 286 cm^{-1}) for Eu^{3+} shown in Fig. 3S,† and the energy gap ΔE^2 (^{3}π–π* to $^5D_0$) of 3547 cm^{-1} falls well within the ideal 2500–4500 cm^{-1} range from Latva's empirical rule,[21] confirming efficient sensitization of the Eu^{3+}-based complex monomer **2**. However, for complex monomer **3**, the small energy gap ΔE^2 (^{3}π–π* to $^5D_4$, 288 cm^{-1}) for Tb^{3+} allows for back energy transfer,[22] giving rise to its dual emissions due to intra-molecular partial energy transfer.

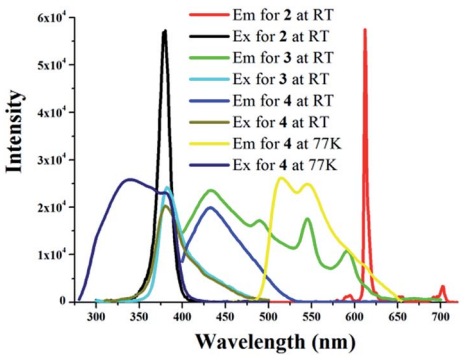

Fig. 2 Emission and excitation spectra (λ_{ex} = 380 nm at RT or λ_{ex} = 339 nm at 77 K) of **2–4** in MeCN solution at 2 × 10^{-5} M.

Synthesis, characterization and photophysical property of homo-Ln^{3+}-grafted polymers Poly(MMA-*co*-1), Poly(MMA-*co*-2), Poly(MMA-*co*-3) and Poly(MMA-*co*-4)

In consideration of the congenital defect of low thermal stability of complex monomers and the excellent performance[23] of the PMMA matrix with low cost, transparency and good mechanical property, each of the complex monomers **2–4** with an active terminal vinyl group was copolymerized with MMA with one stipulated feed molar ratio (100 : 1, 200 : 1, 400 : 1 or 600 : 1) in the presence of AIBN to obtain the series of homo-Ln^{3+}-grafted polymers poly(MMA-*co*-[$Ln(TTA)_3$(4-VB-PBI)) (Ln = Eu, Tb or Gd), respectively. To elucidate their AIBN-assisted free-radical copolymerization,[24] the representative polymer **Poly(MMA-*co*-1)** with a stipulated feed molar ratio of 200 : 1 from the iso-structural and anti-ferromagnetic La^{3+}-based complex monomer **1** was obtained for comparison. With respect to the ^{1}H NMR spectrum of **Poly(MMA-*co*-1)** also shown in Fig. 1S,† besides the combined proton resonances (δ = 8.70–0.93 ppm) of the polymerized complex monomer **1** and MMA, the original three proton resonances of the characteristic vinyl group are unambiguously replaced by two new up-shifted proton resonances (δ = 2.85 and 1.32 ppm) of the –CH and $-CH_2$ groups, confirming the covalent-bonding of complex monomers into the PMMA backbone.[25] Moreover, GPC results (Table 3S†) show that all the polydispersity indices (PDI = M_w/M_n) of these polymers are in the relatively narrow range of 1.17–1.38 due to AIBN-initiated radical copolymerization. It is worth noting that there is an almost linear relationship between the M_n value and the feed molar ratio (100 : 1, 200 : 1, 400 : 1 or 600 : 1) for both **Poly(MMA-*co*-2)** and **Poly(MMA-*co*-3)**, also suggesting a random distribution of complex monomers along the polymeric backbone. Furthermore, the PXRD pattern (Fig. 3) of the representative polymer **Poly(MMA-*co*-2)** (200 : 1) endows only PMMA-based amorphous peaks, also indicating the low-concentration homogeneous distribution[26] of the complex

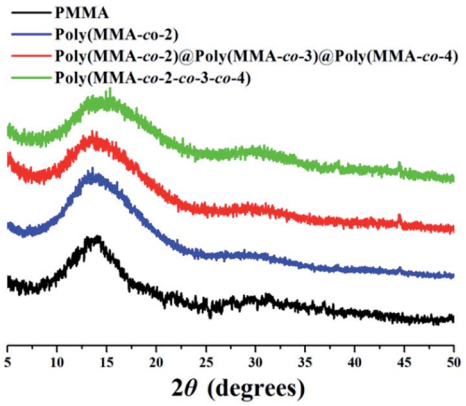

Fig. 3 PXRD patterns of PMMA, **Poly(MMA-*co*-2)** (200 : 1), polymers' blend **Poly(MMA-*co*-2)@Poly(MMA-*co*-2)@Poly(MMA-*co*-2)** (1 : 7 : 8) and Eu^{3+}–Tb^{3+}–Gd^{3+}-grafted polymer **Poly(MMA-*co*-2-*co*-3-*co*-4)** (200 : 1(2/3/4 = 1 : 7 : 8)) in the solid state.

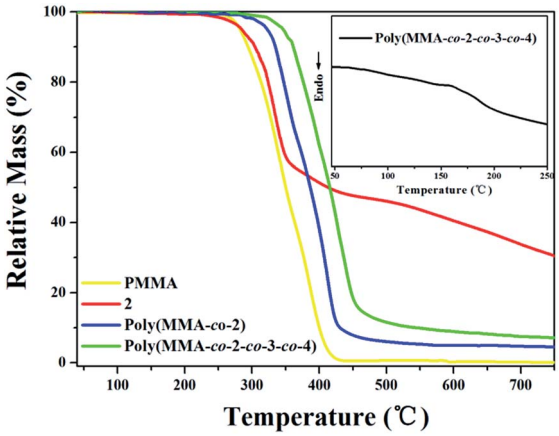

Fig. 4 TG curves of PMMA, complex monomer **2** or polymer **Poly(MMA-*co*-2)** (200 : 1) and TG and DSC (inset) curves of polymer **Poly(MMA-*co*-2-*co*-3-*co*-4)** (200 : 1(2/3/4 = 1 : 7 : 8)) in the solid state.

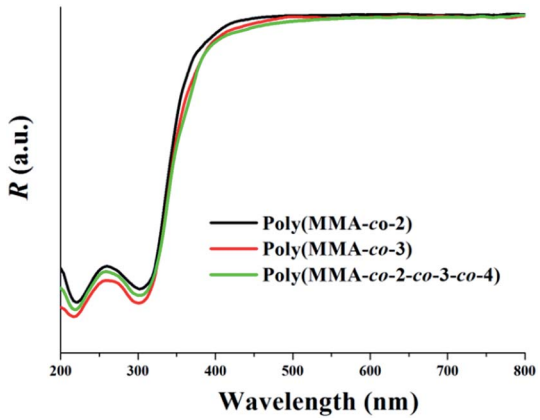

Fig. 5 DR spectra of **Poly(MMA-*co*-2)** (200 : 1), **Poly(MMA-*co*-2)** (200 : 1), polymers' blend **Poly(MMA-*co*-2)@Poly(MMA-*co*-2)@Poly(MMA-*co*-2)** (1 : 7 : 8) and polymer **Poly(MMA-*co*-2-*co*-3-*co*-4)** (200 : 1(2/3/4 = 1 : 7 : 8)) in the solid state at room temperature.

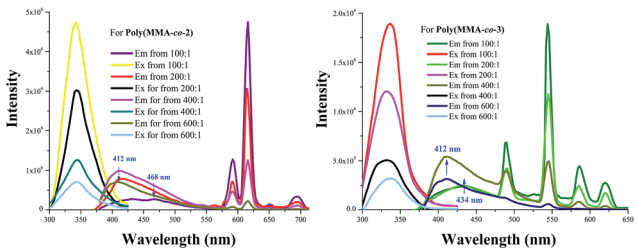

Fig. 6 Emission and excitation spectra (λ_{ex} = 341 nm) of homo-Ln^{3+}-grafted polymers with different feed molar ratios (100 : 1, 200 : 1, 400 : 1 and 600 : 1) in the solid state at room temperature; (**6a**) for **Poly(MMA-*co*-2)**; (**6b**) for **Poly(MMA-*co*-3)**.

monomer **2**. TG analysis (Fig. 4) of **Poly(MMA-*co*-2)** (200 : 1) exhibits a slight increase of 19 °C for the T_{onset} in comparison with pure PMMA, and decomposition with maxima around the higher temperature interval (385–397 °C) than that (310–324 °C) of complex monomer **2**, showing that the thermal stability of **Poly(MMA-*co*-2)** (200 : 1) is significantly improved through copolymerization.

The photophysical properties of polymers **Poly(MMA-*co*-2)** or **Poly(MMA-*co*-3)** with different feed molar ratios (100 : 1, 200 : 1, 400 : 1 and 600 : 1) and **Poly(MMA-co-4)** (200 : 1) were investigated in solid state, and summarized in Fig. 5, 6 and S4.† As shown in Fig. 5, a similar DR spectrum of the PMMA-supported polymer from **2** or **3** at a stipulated feeding molar ratio of 200 : 1 exhibits relatively broader absorption bands than those of **2–4** in solution, where the absorptions at 216–220, 282–284 and 345–349 nm in the UV-visible region should be assigned to electronic transitions from organic moieties of PMMA and the coordinated ligands. Due to the characteristic absorptions of Eu^{3+} or Tb^{3+} commonly appearing above 1000 nm,[27] they are not detected in the corresponding samples. Interestingly, different from the ligands-centered emission (λ_{em} = 434 nm shown in Fig. S4†) for **Poly(MMA-*co*-4)** (200 : 1), both **Poly(MMA-*co*-2)** and **Poly(MMA-*co*-3)** with different feed molar ratios exhibit the corresponding dual-emitting behaviours (Fig. 6) with λ_{ex} = 341 nm, which are similar to that of complex monomer **3** in solution but distinctively different from just Eu^{3+}-centered color-pure red-light of complex monomer **2**. For **Poly(MMA-*co*-2)**, through involvement of low Eu^{3+}-grafting concentration (400 : 1 or 600 : 1), the emission spectrum contains a dominating and uncharacteristically broad emission band centered at 412 nm in addition to the peaks associated with Eu^{3+}-centered emissions, as shown in Fig. 6a. The result of the new band at 412 nm with significant intensity unlikely to originate from pure PMMA (λ_{em} = 390 nm; Fig. 4S†) and distinctively blue-shifted by 22 nm relative to the expected ligands-based emission (λ_{em} = 434 nm; Fig. 4S†) as **Poly(MMA-*co*-4)** (200 : 1), indicates the presence of another species. Actually, when complex monomers of **2** are cast into the PMMA matrix at a feed molar ratio of 400 : 1 or 600 : 1, an intimate spatial wrapping of the flexible PMMA critically confines complex monomers with a high local concentration routinely. In this case, bridging or π–π

stacking between complex monomers is probably essential for generation of the new emission.[28] Noticeably, if grafting the complex monomers **2** at excess concentration (100 : 1), the emission of **Poly(MMA-*co*-2)** regresses to the Eu^{3+}-centered red-light as expected. However, one dissimilar but complementary weak emission composed of ligands-based blue-light (432 nm) and unforeseen red-shifted blue-light (468 nm) due to aggregation-induced exciton formation[29] is observed, from which the **Poly(MMA-*co*-2)** is characteristic of a highly conjugated polymer. In contrast, both the ligands-based blue-light centered at 432 nm and the Eu^{3+}-centered red-light are undisturbed for **Poly(MMA-*co*-2)** with a feed molar ratio of 200 : 1, so this grafting concentration could be supposed to be an optimal dye content despite incomplete energy transfer from the polymeric backbone to Eu^{3+}. Returning to **Poly(MMA-*co*-3)** with different feed molar ratios, all the dual emissions (Fig. 6b) seem similar to those of **Poly(MMA-*co*-2)**, where the ligands-based blue-light (λ_{em} = 434 nm) and the Tb^{3+}-centered green-light are consolidated at a feed molar ratio of 200 : 1 or 100 : 1 without observation of clustering of emitters due to the lower quantum efficiency of complex monomer **3**. In addition, attributed to the PMMA-matrixed substrate with a larger refractive index[30] and recombination of the charge carrier at Eu^{3+}- or Tb^{3+}-related trap sites[31] due to molecular extension for covalently-bonded polymers, the significantly improved luminescent properties for **Poly(MMA-*co*-2)** (200 : 1) or **Poly(MMA-*co*-3)** (100 : 1 and 200 : 1) are further confirmed by longer lifetimes (901 μs for **Poly(MMA-*co*-2)**; 714–721 μs for **Poly(MMA-*co*-3)**) and the relatively larger overall quantum yields (Φ_{em} = 58.4% for **Poly(MMA-*co*-2)**; Φ_{em} = 17.3–21.5% for **Poly(MMA-*co*-3)**) than those of (47.0% or 6.8%) the corresponding complex monomer **2** or **3** in solution, respectively. For this point, by decreasing the grafting content of the incorporated chromophore at a certain level, the clustering of Eu^{3+} or Tb^{3+}-based emitters within could be effectively suppressed.

Synthesis, characterization and color-tunable white-light of polymers' blend of Poly(MMA-*co*-2)@Poly(MMA-*co*-3)@Poly(MMA-*co*-4) and hetero-Ln^{3+}-grafted polymer Poly(MMA-*co*-2-*co*-3-*co*-4)

In consideration of the dual-emitting character of both **Poly(MMA-*co*-2)** (200 : 1) and **Poly(MMA-*co*-3)** (200 : 1) and the fluorescent blue-light (λ_{em} = 434 nm) of **Poly(MMA-*co*-4)** (200 : 1), their simple blending can be expected to be capable of white-light production through simultaneous emission from the three chromophores within. However, as shown in Fig. 7, emission curves for **Poly(MMA-*co*-2)@Poly(MMA-*co*-3)@Poly(MMA-*co*-4)** with different doping mass ratios (1 : 7 : 4, 1 : 7 : 8 and 1 : 7 : 12) do not show the simple addition spectra as expected. At a doping mass ratio of 1 : 7 : 4, although the Gd^{3+}-involved ligands-based blue-light (λ_{em} = 434 nm), Eu^{3+}-centered red-light (λ_{em} = 613 nm) and Tb^{3+}-centered green-light (λ_{em} = 546 nm) are simultaneously emissive, as shown in Fig. 7a, the distinctive suppression of ligands-based blue-light, together with the larger balanced emission intensity of 613 nm ($^7F_2$ of Eu^{3+}) than that of 546 nm ($^7F_5$ of Tb^{3+}), shows an efficient Tb^{3+}-to-Eu^{3+}-containing energy transfer between the interfaced chromophores. This trichromatic integration is responsible for the resultant emitting colors from white-light (points a–b) to purplish-white (points c–e) with variation of the excitation wavelength from 330 to 370 nm. However, the two white-light points (0.367–0.371, 0.320–0.328) are critically deviated from the equal energy point (0.333, 0.333), arising from the deficiency of the ligand-based blue-light. With an increase of relative Gd^{3+}-content in the polymers' blend with a doping mass ratio of 1 : 7 : 8, it is also believed that efficient Tb^{3+} to Eu^{3+} energy transfer takes place by similar domination of the Eu^{3+}-centered emission intensity shown in Fig. 7b. Noticeably, although all the emissive colors (points f–j) almost fall within the white-light region at the whole excitation range of 330–370 nm, the closest to the standard white-light (0.333, 0.333) is located at point g (0.323, 0.298) upon a excitation wavelength of 340 nm. Moreover, besides the slightly higher color corrected temperature (CCT) of 6937 K and the slightly lower CRI of 77 beyond the solid-state lighting requirements (CCT between 2500–6500 and CRI above 80),[32] a quantum yield down to 10.5% is also observed. Furthermore, the three-centered species decay with lifetimes of 4.6 ns from ligands-based blue-light, 934 μs from Eu^{3+}-centered red-light and 478 μs from Tb^{3+}-centered

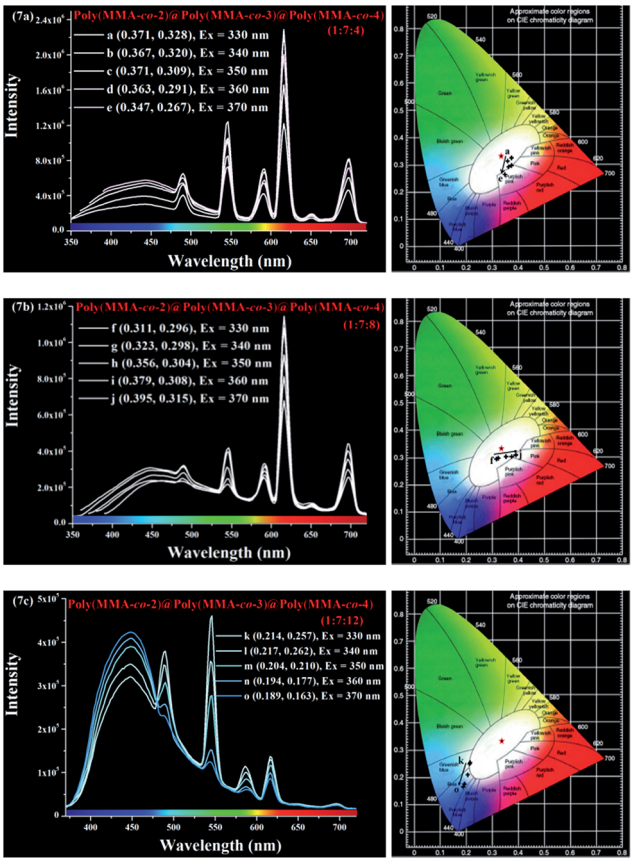

Fig. 7 Emission spectra (left) and corresponding CIE coordinates (right) of polymers' blends Poly(MMA-*co*-2)@Poly(MMA-*co*-2)@Poly(MMA-*co*-2) with different doping mass ratios (1 : 7 : 4, 1 : 7 : 8 and 1 : 7 : 12) in the solid state at room temperature upon excitation: (**7a**) 1 : 7 : 4; (**7b**) 1 : 7 : 8; (**7c**) 1 : 7 : 12.

green-light confirm that the white-light should unambiguously originate from both fluorescence and phosphorescence, and especially, the distinctively decreased Tb^{3+}-centered phosphorescent lifetime (478 μs) than that (714 μs) of **Poly(MMA-*co*-3)** with the same feed molar ratio of 200 : 1 verifies that energy transfer from Tb^{3+} to Eu^{3+} centers indeed takes place. Interestingly, providing further excess **Poly(MMA-*co*-4)** in the blend (1 : 7 : 12), as shown in Fig. 7c, the domination of ligands-based blue-light, together with an unbalanced trichromatic integration, envisions all the resulting emissions beyond the white-light region.

In contrast, with appropriate feed molar ratios (200 : 1[**2**/**3**/**4**] = 1 : 7 : 4, 1 : 7 : 8 and 1 : 7 : 12) *via* doping mass ratios for the copolymerization of MMA and complex monomers **2–4**, one can expect molecular dispersal of different chromophores in a polymeric matrix. More importantly, the low grafting concentration (200 : 1) seems to suggest that the Eu^{3+} and Tb^{3+}-based chromophores involved are effectively separated in the PMMA matrix to inhibit possible Tb^{3+} to Eu^{3+} energy transfer. In particular, blockade of intramolecular energy transfer does not interfere with the sensitization of different chromophores within, from which, their simultaneous emissions can also be expected to be capable of white-light emission. For the representative one (200 : 1[**2**/**3**/**4**] = 1 : 7 : 8) in Eu^{3+}–Tb^{3+}–Gd^{3+}-grafted polymers **Poly(MMA-*co*-2-*co*-3-*co*-4)** (200 : 1[**2**/**3**/**4**] = 1 : 7 : 4, 1 : 7 : 8 and 1 : 7 : 12), similar PXRD, TG and DR results (also in Fig. 3–5) to those of **Poly(MMA-*co*-2)** (200 : 1) are exhibited due to the iso-structural character of complex monomers **2–4**. Especially, its glass-transition temperature (T_g) from the DSC analysis (also in Fig. 4) is about 158 °C, and much higher than those (50–130 °C) of common organic polymers[33] including PMMA (105–128 °C)[34] upon involvement of polymerized complex monomers. Such a high value of T_g should be desirable for Eu^{3+}–Tb^{3+}–Gd^{3+}-grafted polymers used as emissive materials for optoelectronic devices. Moreover, their reasonable PDI values of 1.21–1.24 and M_n values of 19 664–19 725 g mol^{-1} (Table 3S†) are also obtained from the rational AIBN-initiated radical copolymerization of **2–4** and MMA. XPS quantitative analysis also verifies the stoichiometric atomic molar ratios (1 : 6.97 : 3.93, 1 : 7.02 : 7.96 and 1 : 6.98 : 11.95) of Eu^{3+} to Tb^{3+} and to Gd^{3+} as desired feeds ([**2**/**3**/**4** = 1 : 7 : 4, 1 : 7 : 8 and 1 : 7 : 12). As expected, all the polymers **Poly(MMA-*co*-2-*co*-3-*co*-4)** exhibit the simultaneous emissions (Fig. 8) of the Eu^{3+}-centered red-light at 613 nm, Tb^{3+}-centered green-light at 546 nm and the blue-light at 434 nm from the Gd^{3+}-involved ligands, respectively. For **Poly(MMA-*co*-2-*co*-3-*co*-4)** (1 : 7 : 4), as shown in Fig. 8a, even with scarce blue-light, its combination with prominent Eu^{3+}-centered red-light and Tb^{3+}-centered green-light gives rise to the emitting colors (points A–E) falling well within the white-light region upon excitation from 345 nm to 365 nm. Of particular note, excitation at 360 nm is found to produce a high-quality white-light emission (point D): a CIE coordinate of $x = 0.346$, $y = 0.319$; a CCT of 4769 K and the CRI up to 85. To our dismay, a relatively lower overall white-light quantum yield (9.6%) comparable with that (10.5%) of the optimal point *g* for the polymers' blend is also obtained because it is saturated from a longer excitation wavelength (360 nm)

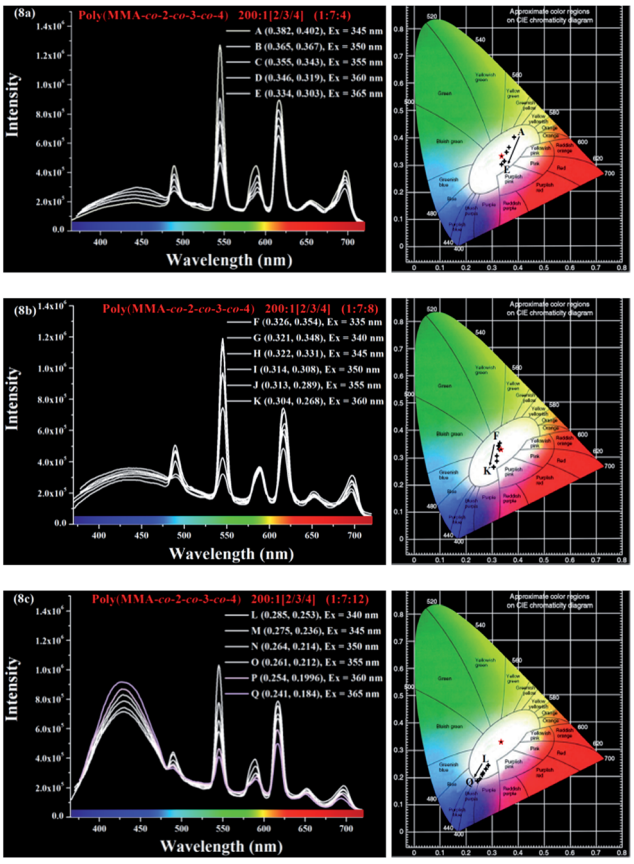

Fig. 8 Emission spectra (left) and corresponding CIE coordinates (right) of Eu^{3+}–Tb^{3+}–Gd^{3+}-grafted polymers **Poly(MMA-*co*-2-*co*-3-*co*-4)** in the solid state at room temperature upon excitation: (**8a**) 200 : 1(**2**/**3**/**4** = 1 : 7 : 4); (**8b**) 200 : 1(**2**/**3**/**4** = 1 : 7 : 8); (**8c**) 200 : 1(**2**/**3**/**4** = 1 : 7 : 12).

deviated from 341 nm (λ_{ex}). Nonetheless, the results of almost constant Eu^{3+}- or Tb^{3+}-centered phosphorescent lifetime (903 μs or 718 μs) as comparable with that (901 μs or 714 μs) of **Poly(MMA-*co*-2)** (200 : 1) or **Poly(MMA-*co*-3)** (200 : 1) should be the reason for their uniform dispersal in the PMMA chain. Thus, through contact in the interface mainly between PMMA and chromophores, Tb^{3+} to Eu^{3+} centers' energy transfer is effectively inhibited. After supplementation of insufficient blue-light, the perfect trichromatic incorporation renders all the resultant emissions characteristic of white-light as desired for **Poly(MMA-*co*-2-*co*-3-*co*-4)** (1 : 7 : 8), as shown in Fig. 8b. In contrast to **Poly(MMA-*co*-2-*co*-3-*co*-4)** (1 : 7 : 4), the highest-quality white-light (point H; 0.322, 0.331) is more close to the ideal white-light, and the CCT of 5979 K between 2500–6500 and an ultra-high CRI of 94 are estimated. More importantly, the optimal white-light is produced at a relatively shorter excitation wavelength of 345 nm besides the similar resource of both fluorescence (6.3 ns) and phosphorescence (897 μs of Eu^{3+}-center and 717 μs of Tb^{3+}-center). This wavelength is very near to 341 nm (λ_{ex}) of the three chromophores within, affording a large quantum yield up to 17.8%, which is the highest among all reported white-light-emitting polymeric systems with Ln^{3+}-doping[9] or Ln^{3+}-grafting[12a,12b,12c,15] from the RGB trichromatic

strategy, and comparable with the best (18.4% or 20.4%) of Ln^{3+}-related polymers[12d] or MOFs[35] by the dichromatic strategy. Similarly, further increase in the relative Gd^{3+}-content in formation of **Poly(MMA-*co*-2-*co*-3-*co*-4)** (1 : 7 : 12), the excess Gd^{3+}-incorporated blue-light leads to the low-quality white-light shown in Fig. 8c, where a distinct tendency approaching bluish-purple of their CIE coordinates (0.241–0.285, 0.184–0.253; points L–Q) upon excitation from 340 to 365 nm is exhibited.

Conclusions

For the first example of the single-component Eu^{3+}–Tb^{3+}–Gd^{3+}-grafted polymer **Poly(MMA-*co*-2-*co*-3-*co*-4)**, the color-tuning to direct high-quality white-light (CIE coordinate of $x = 0.322$, $y = 0.331$; CCT of 5979 K and ultra-high CRI of 94) can be realized readily from judicious adjustments of both the Eu^{3+}–Tb^{3+}–Gd^{3+} concentration and excitation wavelength. In particular, through control of an optimal grafting concentration, we provide a conceptual strategy to effectively suppress Tb^{3+} to Eu^{3+} energy transfer or exciton formation for hetero-Ln^{3+}-grafted polymers. Moreover, the superior physical properties, including a high luminous efficiency of 17.8% and an ultra-high CRI of 94 for **Poly(MMA-*co*-2-*co*-3-*co*-4)** (1 : 7 : 8), suggest that it could be used in color-critical high-level applications.

Acknowledgements

The authors acknowledge funds from the National Natural Science Foundation (21373160, 91222201, 21173165), the Program for New Century Excellent Talents in University from the Ministry of Education of China (NCET-10-0936), the Doctoral Program (20116101110003) of Higher Education, the Science, Technology and Innovation Project (2012KTCQ01-37) of Shaanxi Province, the Graduate Innovation and Creativity Fund (YZZ15036) of Northwest University in P. R. of China, and the Robert A. Welch Foundation (F-816).

Notes and references

1 (*a*) P. Waltereit, O. Brandt, A. Tramper, H. T. Grahn, J. Menniger, M. Ramsteiner, M. Reiche and K. H. Ploog, *Nature*, 2000, **406**, 865–868; (*b*) H. Sasabe and J. Kido, *J. Mater. Chem. C*, 2013, **1**, 1699–1707; (*c*) C. Xu and K. M. Podusha, *J. Mater. Sci.*, 2015, **26**, 4565–4570; (*d*) J. Meyer and F. Tappe, *Adv. Opt. Mater.*, 2015, **3**, 424–430.

2 T. R. Kuykendal, A. M. Schwartzberg and S. Aloni, *Adv. Mater.*, 2015, **27**, 5805–5812.

3 Q. Zhang, C.-F. Wang, L.-T. Ling and S. Chen, *J. Mater. Chem. C*, 2014, **2**, 4358–4373.

4 (*a*) K. T. Kamtekar, A. P. Monkman and M. R. Bryce, *Adv. Mater.*, 2010, **22**, 572–582; (*b*) G. M. Farinola and R. Ragni, *Chem. Soc. Rev.*, 2011, **40**, 3467–3482; (*c*) H. Sasabe and J. Kido, *Eur. J. Org. Chem.*, 2013, 7653–7663; (*d*) L. Bao and M. D. Heagy, *Curr. Org. Chem.*, 2014, **18**, 740–772; (*e*) S. Mukherjee and P. Thilagar, *Dyes Pigm.*, 2014, **110**, 2–27.

5 C. Tang, X.-D. Liu, F. Liu, X.-L. Wang, H. Xu and W. Huang, *Macromol. Chem. Phys.*, 2013, **214**, 314–342.

6 (*a*) C.-L. Ho and W.-Y. Wong, *New J. Chem.*, 2013, **37**, 1665–1683; (*b*) C. Fan and C. Yang, *Chem. Soc. Rev.*, 2014, **43**, 6439–6469.

7 (*a*) L. Ying, C.-L. Ho, H. Wu, Y. Cao and W.-Y. Wong, *Adv. Mater.*, 2014, **26**, 2459–2473; (*b*) X. Yang, G. Zhou and W.-Y. Wong, *J. Mater. Chem. C*, 2014, **2**, 1760–1778; (*c*) J. Xiang, C.-L. Ho and W.-Y. Wong, *Polym. Chem.*, 2015, **6**, 6905–6930.

8 (*a*) P. Coppo, M. Duati, V. N. Kozhevnikov, J. W. Hofstraat and L. de Cola, *Angew. Chem., Int. Ed.*, 2005, **44**, 1806–1810; (*b*) G.-L. Law, K.-L. Wong, H.-L. Tam, K.-W. Cheah and W.-T. Wong, *Inorg. Chem.*, 2009, **48**, 10492–10494.

9 (*a*) N. T. Kalyani and S. J. Dhoble, *Renewable Sustainable Energy Rev.*, 2012, **16**, 2696–2723; (*b*) L.-J. Xu, G.-T. Xu and Z.-N. Chen, *Coord. Chem. Rev.*, 2014, **273–274**, 47–62.

10 (*a*) S. Roy, A. Chakraborty and T. K. Maji, *Coord. Chem. Rev.*, 2014, **273–274**, 139–164; (*b*) J. Wu, H. Zhang and S. Du, *J. Mater. Chem. C*, 2016, **4**, 3364–3374; (*c*) Y. Cui, B. Li, H. He, W. Zhu, B. Chen and G. Qian, *Acc. Chem. Res.*, 2016, **49**, 483–493.

11 J. M. Stanley and B. J. Holliday, *Coord. Chem. Rev.*, 2012, **256**, 1520–1530.

12 (*a*) Y. S. L. V. Narayana, S. Basal, M. Baumgarten, K. Müllen and R. Chandrasekar, *Adv. Funct. Mater.*, 2013, **23**, 5875–5880; (*b*) S. Basak, Y. S. L. V. Narayana, M. Baumgarten, K. Müllen and R. Chandrasekar, *Macromolecules*, 2013, **36**, 362–369; (*c*) Y. S. L. V. Narayana, S. Basal, M. Baumgarten, K. Müllen and R. Chandrasekar, *Macromolecules*, 2015, **48**, 4801–4812; (*d*) Z. Zhang, Y.-N. He, L. Liu, X.-Q. Lü, X.-J. Zhu, W.-K. Wong, M. Pan and C.-Y. Su, *Chem. Commun.*, 2016, **52**, 3713–3716.

13 J. Silver, R. Withnall and A. Kitai, *Luminescent Materials and Applications*, John Wiley & Sons, Chicester, 2008, p. 75.

14 (*a*) R. Shunmugam and G. N. Tew, *J. Am. Chem. Soc.*, 2005, **127**, 13567–13572; (*b*) R. Shunmugam and G. N. Tew, *Macromol. Rapid Commun.*, 2008, **29**, 1355–1362.

15 A. Zhang, N. Sun, L. Li, Y. Yang, X. Zhang, H. Jia, X. Kiu and B. Xu, *J. Mater. Chem. C*, 2015, **3**, 9933–9941.

16 G. Xiang, S. Lin, W. Cui, L. Wang, L. Zhou, L. Li and D. Cao, *Sens. Actuators, B*, 2013, **188**, 540–547.

17 P. A. Vigato, V. Peruzzo and S. Tamburini, *Coord. Chem. Rev.*, 2009, **253**, 1099–1201.

18 H. Xu, Q. Su, Z.-F. An, Y. Wei and X.-G. Liu, *Coord. Chem. Rev.*, 2015, **293–294**, 228–249.

19 S. V. Eliseeva and J.-C. G. Bünzli, *Chem. Soc. Rev.*, 2010, **39**, 189–227.

20 F. J. Steemers, W. Verboom, D. N. Reinhoudt, E. B. Van der Tol and J. W. Verhoeven, *J. Am. Chem. Soc.*, 1995, **117**, 9408–9414.

21 M. Latva, H. Mukkala, C. Matachescu, J. C. Rodriguez-Ubis and J. Kanakare, *J. Lumin.*, 1997, **175**, 149–169.

22 D. Sykes, A. J. Cankut, N. M. Ali, A. Stephenson, S. J. P. Spall, S. C. Parker, J. A. Weinstein and M. D. Ward, *Dalton Trans.*, 2014, **43**, 6414–6428.

23 (*a*) W.-Q. Fan, J. Feng, S.-Y. Song, Y. Lei, G.-L. Zhang and H.-J. Zhang, *Chem.–Eur. J.*, 2010, **16**, 1903–1910; (*b*) S. Biju, Y. K. Eom, J.-C. G. Bünzli and H. K. Kim, *J. Mater. Chem. C*, 2013, **1**, 6935–6944.

24 Y. Nakamura, Y. Kitada, Y. Kobayashi, B. Ray and S. Yamago, *Macromolecules*, 2011, **44**, 8388–8397.
25 T.-Z. Miao, W.-X. Feng, Z. Zhang, P.-Y. Su, X.-Q. Lü, J.-R. Song, D.-D. Fan, W.-K. Wong, R. A. Jones and C.-Y. Su, *Eur. J. Inorg. Chem.*, 2014, 2839–2848.
26 Z. Zhang, W.-X. Feng, P.-Y. Su, X.-Q. Lü, J.-R. Song, D.-D. Fan, W.-K. Wong, R. A. Jones and C.-Y. Su, *Inorg. Chem.*, 2014, **53**, 5950–5960.
27 V. Vicinelli, P. Ceroni, M. Maestri, V. Balzani, M. Gorka and F. Vögtle, *J. Am. Chem. Soc.*, 2002, **124**, 6461–6468.
28 B. D. Alleyne, L. A. Hall, I. A. Kahwa, A. J. P. Andrew and D. J. Williams, *Inorg. Chem.*, 1999, **38**, 6278–6284.
29 A. H. Shelton, I. V. Sazanovich, J. A. Weinstein and M. D. Ward, *Chem. Commun.*, 2012, **48**, 2749–2751.
30 J. Kai, M. C. F. C. Felinto, L. A. O. Nunes, O. L. Malta and H. F. Brito, *J. Mater. Chem.*, 2011, **21**, 3796–3802.
31 P. Martin-Ramos, V. Lavín, M. Ramos Silva, I. R. Martín, F. Lahoz, P. Chamorro-Posada, J. A. Paixão and J. Martín-Gil, *J. Mater. Chem. C*, 2013, **1**, 5701–5710.
32 (*a*) B. W. D'Andrade and S. R. Forrest, *Adv. Mater.*, 2004, **16**, 1585–1595; (*b*) M. Shang, C. Li and J. Lin, *Chem. Soc. Rev.*, 2014, **43**, 1372–1386.
33 Y. Jin, J. Y. Kim, S. H. Park, J. Kim, S. Lee, K. Lee and H. Suh, *Polymer*, 2005, **46**, 12158–12165.
34 P. D. Condo, D. R. Paul and K. P. Johnston, *Macromolecules*, 1994, **27**, 365–371.
35 C.-Y. Su, X.-L. Wang, X. Zhang, C. Qin, P. Li, Z.-M. Su, D.-X. Zhu, G.-G. Shan, K.-Z. Shao, H. Wu and J. Li, *Nat. Commun.*, 2013, **4**, 3717.